Evaluation of different high frequency EOP models using VLBI

Tobias Nilsson
Latmäteriet, Gävle, Sweden
jan-tobias.nilsson@lm.se

November 16, 2018

1 Summary

In this memo I present the results of my evaluation of the various model considered by the IERS working group on HF-EOP as a possible future conventional model for the high frequency EOP variations. The evaluation has been done with VLBI using all R1, R4 and CONT sessions from the period 2007-2016. Firstly, all data was used to study how well the models explain the EOP variations in the diurnal and semi-diurnal frequency bands. Secondly, the data from the CONT campaigns (including also the most recent on, CONT17) was used to estimate polar motion and UT1-UTC with hourly resolution, and these time series were then compared to the model predictions.

2 Data analysis

The VLBI data were analysed with the VieVS@GFZ software, version G2018.7. For the a priori modelling I followed the IERS Conventions [Petit and Luzum, 2010], except that I also corrected for non-tidal atmospheric, ocean, and hydrological loading. For each session, I estimated station coordinates, radio source coordinates, tropospheric parameters, clocks, and EOP (for the exact parametrization, see below).

3 Evaluated models

In this work, I investigate the models given in Table 1. The tables of the coefficiaents for the respective models were obtained for the web-site of the working group (`https://ivscc.gsfc.nasa.gov/hfeop_wg/`.The effect of libration were corrected using the models in the IERS Conventions, except for the ABN models which (to my knowledge) contain also these effects.

4 Results

4.1 VLBI sessions 2007-2016

Here I first present some results from the analysis of all R1, R4, and CONT sessions from the period 2007-2016 (1072 sessions).

4.1.1 Weighed RMS of the residuals

I first investigated how how the post-fit residuals were affected by applying the different high frequency EOP models a priori. I made a standard VLBI analysis, estimating all EOP with daily

Table 1: List of the different high frequency EOP models considered in this work. The first six are all based on various ocean tide models, while the last three are empirical models from VLBI aor VLBI+GPS data.

Model	Based on	Reference
IERS	TPXO4	Petit and Luzum [2010]
Desai	TPXO8	Desai and Sibois [2016]
EOT11a	EOT11a	Karbon et al. [2018]
FES2012	FES2012	Karbon et al. [2018]
HAMTIDE	HAMTIDE	Karbon et al. [2018]
Madzak	EOT11a	Madzak et al. [2016]
Gipson	VLBI data	Updated version of Gipson and Hesslow [2015]
ABN VLBI	VLBI data	Böckmann and Nothnagel [2011]
ABN Comb.	VLBI and GPS	Artz et al. [2012]

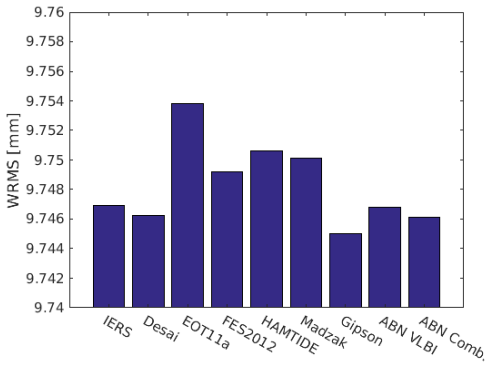

Figure 1: WRMS of the post-fit residuals obtained when different high frequency EOP models are applied a priori.

resolution, and applying the differnt high frequency EOP models a priori. Then, for each model I calculated the weighted RMS (WRMS) of the post-fit residuals over all sessions. The results can be seen in Fig. 1. It can be seen that the WRMS of the residuals are hardly affected by the applied high frequency EOP model; the differences are on the μm level. The reason is that the high frequency EOP model has only limited effect on the residulats, much more important are other factors as, e.g., the observation noise. Hence, no strong conclusions can be drawn from these results. Nevertheless, since the only difference between the analyses was the applied high frequency EOP model, the differences are only due to the models applied. The lowest WRMS is obtained for the Gipson model, followed by ABN Combined and the Desai models.

4.1.2 Admittance factors

Secondly, I also estimated admittance factors for the different models. The admittance factors give indication on whether the model generally under- or over-estimates the amplitudes of the variations. If the model is correct, the admittance factor should be equal to 1. However, it is not obvious that an admittance factor close to 1 means that the model is good.

In the data analysis I set up the admittance factors for each session. Then, I combined all sessions in a global solution, where the admittance factors were estimated as global parameters and all other parameters were estimated as session-wise parameters. I calculated two different solution, In the first individual admittance factors for polar motion and UT1-UTC were estimated, in the second I only estimated one admittance factor valid for all EOP. The results can be seen in Fig. 2. It can be noted that the empirical models (Gipson and the two ABN models) all give admittance factors close to 1 for UT1-UTC. Their results for polar motion and overall are also rather good.

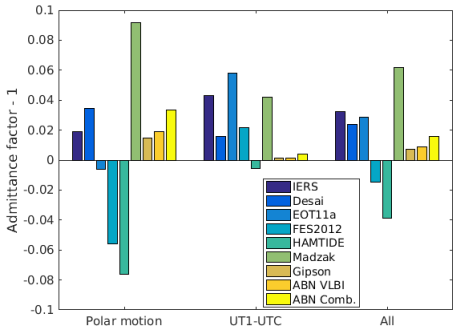

Figure 2: Admittance factors estimated for the different high frequency EOP models. Shown are the individual admittance factors for polar motion and UT1-UTC, respectively, as well as common admittance factors for both.

EOT11a have an admittance factor close to 1 for polar motion, but not for UT1-UTC. The opposite is the case for the HAMTIDE model.

4.1.3 Diurnal and semi-diurnal amplitudes

The method for evaluation used here is inspired by the method of Complex Demodulations [Brzeziński, 2012]. Basically, the high frequency EOP variations are all expected to have variations in the diurnal and semi-diurnal bands, and the tested model in principle only contains terms in these bands. If we consider a short period, like on day (the length of a typical VLBI session), a signal with a frequency close to 1 cpd (or 2 cpd) can be approximated pretty well by a signal having the exact frequency 1 cpd (2 cpd). Thus, one way to handle possible errors in the high frequency EOP models in the VLBI analysis, would be to estimate also diurnal and semi-diurnal EOP terms in addition to the daily EOP and EOP rates usually estimated. Furthermore, if this is done one can look at the amplitudes of the estimated diurnal and semi-diurnal EOP variations to check the accuracy of the high frequency EOP model used: if the model is good the estimated amplitudes should be small.

To test the EOP high frequency models using this method, I estimated for each session offsets and drifts as well as diurnal and semi-diurnal terms for x-pole, y-pole, and UT1-UTC. Nutation was fixed to the a priori values since it would be impossible to separate nutation offsets from retrograde diurnal polar motion terms in the analysis. I would, however, expect this to have little impact on the results since the nutation errors should be completely estimated as retrograde diurnal polar motion, which is not considered in the following study.

Figure 3 shows the weighted mean of the estimated amplitudes of retrograde semi-diurnal polar motion, prograde and semi-diurnal and diurnal polar motion, as well as semi-diurnal and diurnal UT1-UTC. This figure shows the results when using the different high frequency EOP models as a priori, as well as the case when no a priori model was used. It is rather obvious that not using any model gives significantly higher amplitudes.

A little bit more detailed view of the performance of the model is shown in Fig. 4. Furthermore, the weighted mean amplitudes for each frequency band are listed in Table 2, together with the weighted mean amplitudes for polar motion, UT1-UTC, and of all amplitudes. We can note that the mean amplitudes are rather similar for all models. This is probably because the estimated amplitudes are also influenced by non-tidal sub-diurnal EOP variations as well as observation noise, both of which are not described by the models. Nevertheless, both these effects should be uncorrelated with the model errors, thus we can expect that the best models should give the lowest amplitudes. For polar motion we can note that the lowest mean amplitudes, as well as the smallest variations between the models, are seen in the prograde semi-diurnal band (+12 h). It seems the performance of all models are similar in this band. In the prograde diurnal, and especially in the

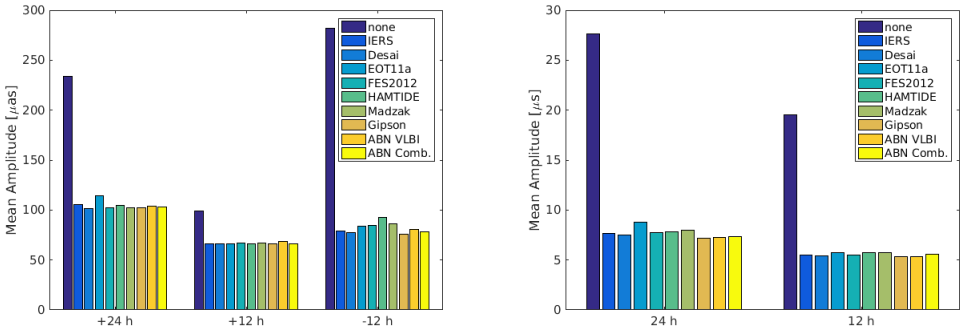

Figure 3: Weighted mean of the estimated diurnal and sub-diurnal polar motion (left) and UT1-UTC (right) amplitudes, obtained when applying different high frequency EOP models a priori, as well as when using no model at all.

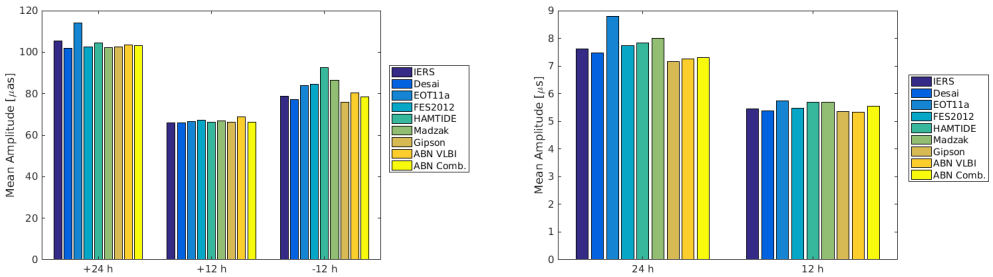

Figure 4: Weighted mean of the estimated diurnal and sub-diurnal polar motion (left) and UT1-UTC (right) amplitudes, obtained when applying different high frequency EOP models a priori.

retrograde semi-diurnal band, we can seen more variations between the models. In total, the best model for polar motion seems to be the one from Gipson, followed closely by the Desai model. The Gipson model also have the best results for UT1-UTC, closely followed by the other empirical VLBI model, ABN VLBI. Out of the models based on ocean tide models, the Desai model has the best results for UT1-UTC. In total, the best results are obtained for the Gipson model, followed by the Desai model.

4.2 Hourly EOP from the CONT campaigns

The CONT campaigns are special, 15-day long, VLBI campaigns performed about every third years to demonstrate the current state-of-the-art of geodetic VLBI. One of the aim of these campaign is to estimate EOP with sub-daily temporal resolution. Numerous studies have used the CONT campaigns to study high frequency EOP variations and have demonstrated that these data are good for this purpose. Thus, the CONT campaigns are excellent data sets for testing high frequency EOP models.

I analysed the data from the past four CONT campaigns: CONT08 (August 2008), CONT11 (September 2011), CONT14 (May 2014), and CONT17 (November-December 2017). In the CONT17 campaigns there were three different VLBI networks observing independently, two legacy networks sand one network of new VGOS antennas (the VGOS network only observed for 5 days). For the results presented in this section I have combined the solutions of the two legacy network (denoted as CONT17), while the VGOS network is presented separately (denoted as VGOS17). I estimated polar motion and UT1-UTC with hourly resolution. To get a higher precision for the EOP, all sessions of each CONT campaign was combined i a global solution, estimating one

Table 2: Weighted mean of the estimated diurnal and sub-diurnal polar motion (left) and UT1-UTC (right) amplitudes, obtained when applying different high frequency EOP models a priori. Shown are the results for the considered frequency bands,the mean amplitudes of polar motion and UT1-UTC, as well as the overall mean amplitudes. The smallest and largest values in each column are marked in blue and red, respectively.

	Polar motion				UT1-UTC			Total
Model	+24 h	+12 h	-12 h	Total	24 h	12 h	Total	
	[μas]	[μas]	[μas]	[μas]	[μs]	[μs]	[μs]	[μas]
IERS	105.5	65.8	78.8	75.7	7.63	5.46	6.26	82.4
Desai	101.7	66.0	77.0	74.6	7.48	5.38	6.16	81.2
EOT11a	113.9	66.6	84.1	79.2	8.79	5.73	6.86	88.0
FES2012	102.6	67.1	84.7	78.6	7.74	5.46	6.31	84.5
HAMTIDE	104.5	66.2	92.5	81.9	7.83	5.70	6.48	87.5
Madzak	102.2	66.8	86.5	79.2	7.99	5.70	6.53	86.1
Gipson	102.4	66.3	75.9	74.3	7.17	5.36	6.02	80.2
ABN VLBI	103.5	68.9	80.3	77.6	7.27	5.32	6.04	82.3
ABN Comb.	103.3	66.3	78.5	75.6	7.31	5.56	6.20	81.9

Table 3: WRMS difference between the EOP time series and the high frequency EOP models calculated over all CONT campaigns. Shown are the results for x-pole, y-pole, polar motion (i.e. both x-pole and y-pole), UT1-UTC, and all EOP (x-pole, y-pole, and UT1-UTC combined). The smallest and largest values in each column are marked in blue and red, respectively.

Model	x-pole	y-pole	PM	UT1-UTC	Total
	[μas]	[μas]	[μas]	[μs]	[μas]
IERS	107.1	114.0	110.4	7.66	111.9
Desai	105.4	110.4	107.8	7.57	109.8
EOT11a	114.5	119.9	117.1	8.60	121.2
FES2012	110.7	113.4	112.0	7.63	112.8
HAMTIDE	111.3	120.4	115.7	7.88	116.6
Madzak	112.3	114.7	113.5	8.03	115.9
Gipson	105.5	111.1	108.2	7.25	108.4
ABN VLBI	107.1	115.2	111.0	7.41	111.1
ABN Comb.	106.7	110.5	108.5	7.33	109.0

set of station and radio source coordinates for the whole campaign. I also filtered the obtained EOP time series to remove the low frequency (period >2 days) variations as well as the retrograde diurnal polar motion (since this is by convention nutation).

As a first simple test of the models, I calculated the WRMS difference between the estimated EOP time series from the CONT campaigns and the various high frequency EOP models. The results when using the data from all campaigns is shown in Table 3. We can note that the Desai model gives the lowest WRMS differences for polar motion, followed by the Gipson model. For UT1-UTC the lowest WRMS values are found for the the empirical models, with the Gipson model performing best. Among the other models the Desai has the lowest WRMS. Overall, the lowest WRMS values are found for the Gipson model, followed closely by the ABN Combined and the Desai models.

The WRMS values for the individual campaigns can be seen in Tables 4–8. Although there are some differences between the campaigns, in general it can be seen that the best performing models are the Gipson model, the two ABN models, as well as the Desai model. The only real exception is the VGOS17 campaign. However, since this campaign was only five days long, only five stations, and consisted of a new observing system, the results are not too reliable.

Furthermore, I subtracted each model from the estimated EOP time series and calculated the

spectra of the residual EOP variations. The results can be seen in Figs. 5–9. It can be seen that there are commonly peaks at around 12 h and 24 h, showing that the models are not perfectly describing all sub-diurnal variations in the EOP series. Furthermore, the amplitudes of these peaks are different between the models. At other periods all models give almost identical results, which is expected since the models in principle only contain variations around 12 h and 24 h periods. It can be noted that the models give similar results for the prograde semi-diurnal polar motion peaks confirming the earlier finding that the models perform similar in this band. For the other peaks, there are bigger differences. For example, it can be noted that the EOT11a model seems to have large peaks at +24 h, both in polar motion and UT1-UTC, indicating that this model has problems for this frequency. The model having the smallest peaks varies between the frequency bands and the different CONT campaigns. However, in general it is found that the Gipson and Desai models are usually among those with the smallest peaks.

5 Conclusions

The best performing model is varying dependent on what metric is used and what parameter is investigated. However, in all the investigations I have done in this work, the Gipson and Desai models tends to be among the best in all cases. The other empirical models, ABN VLBI and ABN Combined, are also doing well. If I try to summarize all results, I would say that the best model is the Gipson model, followed closely by the Desai model and the two ABN models. If I only look at polar motion, there is a close call between the Desai or the Gispon models, however, for for UT1-UTC the empirical models, particularly the Gispon model are better. If I only would consider the models base on an ocean tide model, I find that the Desai model is the best one.

However, it should be pointed out that the empirical models are derived from VLBI data (ABN Combined in combination with GNSS, Gipson and ABN VLBI only from VLBI), and that the data used to derive these models are at least partly overlapping with the data I used in this evaluation. Thus, it is likely that the results of these models are biased by this fact. Considering this fact, the Desai model would be the preferred one based on this study, since it performed alsmost as good as the Gipson model overall but is not based on VLBI data.

References

T. Artz, L. Bernhard, A. Nothnagel, P. Steigenberger, and S. Tesmer. Methodology for the combination of sub-daily Earth rotation from GPS and VLBI observations. *J. Geodesy*, 86: 221–239, 2012. doi: 10.1007/s00190-011-0512-9.

T. Artz S. Böckmann and A. Nothnagel. Assessment of periodic sub-diurnal Earth orientation parameter variations at tidal frequencies via transformation of VLBI normal equation systems. *J. Geodesy*, 85(9):565–584, 2011. doi: 10.1007/s00190-011-0457-z.

A. Brzeziński. On estimation of high frequency geophysical signals in Earth rotation by complex demodulation. *J. Geodyn.*, 62:74–82, 2012. doi: 10.1016/j.jog.2012.01.008.

S. D. Desai and A. E. Sibois. Evaluating predicted diurnal and semidiurnal tidal variations in polar motion with GPS-based observations. *J. Geophys. Res.*, 121(7):5237–5256, 2016. doi: 10.1002/2016JB013125.

J. Gipson and L. Hesslow. A new model of HF-EOP variation derived from 35 years of VLBI. *Geophys. Res. Abstracts*, 17, 2015. EGU2015-14756.

M. Karbon, K. Balidakis, S. Belda, T. Nilsson, J. Hagedoorn, and H. Schuh. Long-term evaluation of ocean tidal variation models of polar motion and UT1. *Pure and Applied Geophysics*, 2018. doi: 10.1007/s00024-018-1866-1. in press.

Table 4: Same as Table 3, but only for the CONT08 campaign.

Model	x-pole [μas]	y-pole [μas]	PM [μas]	UT1-UTC [μs]	Total [μas]
IERS	121.2	115.9	118.6	8.92	125.7
Desai	120.0	111.0	115.6	8.83	123.5
EOT11a	125.2	116.9	121.1	10.22	136.6
FES2012	125.3	110.6	118.3	9.02	126.3
HAMTIDE	127.3	120.0	123.7	9.17	130.2
Madzak	121.6	115.2	118.5	9.31	128.5
Gipson	120.0	110.7	115.5	8.33	119.9
ABN VLBI	118.3	111.5	115.0	8.37	119.9
ABN Comb.	118.0	108.8	113.5	8.46	119.8

Table 5: Same as Table 3, but only for the CONT11 campaign.

Model	x-pole [μas]	y-pole [μas]	PM [μas]	UT1-UTC [μs]	Total [μas]
IERS	111.3	127.5	119.2	10.13	119.6
Desai	110.0	123.8	116.7	10.00	117.0
EOT11a	127.6	137.7	132.5	10.81	132.8
FES2012	120.6	129.9	125.1	10.41	125.4
HAMTIDE	117.8	135.5	126.6	10.08	126.8
Madzak	119.0	127.9	123.3	10.21	123.6
Gipson	110.7	125.1	117.8	9.72	118.0
ABN VLBI	109.3	123.4	116.2	9.91	116.6
ABN Comb.	114.4	122.8	118.5	9.93	118.8

M. Madzak, M. Schindelegger, J. Böhm, W. Bosch, and J. Hagedoorn. High-frequency Earth rotation variations deduced from altimetry-based ocean tides. *J. Geodesy*, 90(11):1237–1253, 2016. doi: 10.1007/s00190-016-0919-4.

G. Petit and B. Luzum, editors. *IERS Conventions (2010)*. IERS Technical Note 36. Verlag des Bundesamts für Kartographie und Geodäsie, Frankfurt am Main, Germany, 2010.

Table 6: Same as Table 3, but only for the CONT14 campaign.

Model	x-pole [μas]	y-pole [μas]	PM [μas]	UT1-UTC [μs]	Total [μas]
IERS	101.1	102.9	101.9	7.00	103.1
Desai	101.3	98.9	100.2	6.88	101.3
EOT11a	105.7	110.5	107.9	7.78	111.2
FES2012	101.1	104.9	102.9	6.73	102.2
HAMTIDE	100.6	111.5	105.7	7.14	106.3
Madzak	110.8	104.5	107.9	7.49	109.5
Gipson	100.9	102.7	101.7	6.62	100.9
ABN VLBI	105.4	110.4	107.8	6.80	105.7
ABN Comb.	102.4	101.9	102.2	6.70	101.6

Table 7: Same as Table 3, but only for the CONT17 campaign.

Model	x-pole [μas]	y-pole [μas]	PM [μas]	UT1-UTC [μs]	Total [μas]
IERS	97.5	113.1	105.2	7.15	106.0
Desai	93.2	110.3	101.6	7.16	103.8
EOT11a	103.7	118.0	110.7	7.96	114.0
FES2012	99.7	110.1	104.7	7.27	106.3
HAMTIDE	102.8	117.4	109.9	7.56	111.2
Madzak	100.0	115.1	107.4	7.44	108.9
Gipson	94.0	108.5	101.1	6.87	101.8
ABN VLBI	97.2	116.7	106.8	7.11	106.8
ABN Comb.	94.6	109.8	102.0	6.88	102.5

Table 8: Same as Table 3, but only for the VGOS17 campaign.

Model	x-pole [μas]	y-pole [μas]	PM [μas]	UT1-UTC [μs]	Total [μas]
IERS	175.8	113.3	142.7	7.80	129.4
Desai	170.9	116.7	141.8	7.12	124.0
EOT11a	166.4	98.0	130.9	8.08	125.7
FES2012	185.7	113.1	147.7	7.28	128.2
HAMTIDE	195.1	122.4	156.8	6.71	129.2
Madzak	163.3	100.3	130.3	7.68	122.3
Gipson	162.7	111.3	135.1	7.39	122.5
ABN VLBI	162.6	104.3	131.8	7.84	124.2
ABN Comb.	167.3	117.1	140.2	7.54	126.1

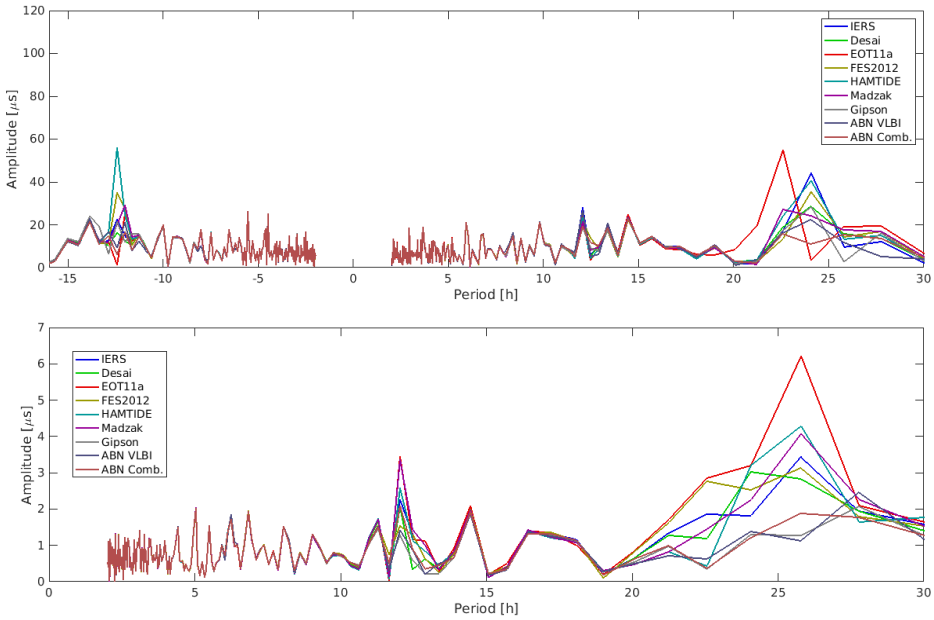

Figure 5: Spectra of the residual polar motion ($p = x_p - i\,y_p$, top) and UT1-UTC (bottom variations after the various models have been removed from the estimated EOP time series from the CONT08 campaign.

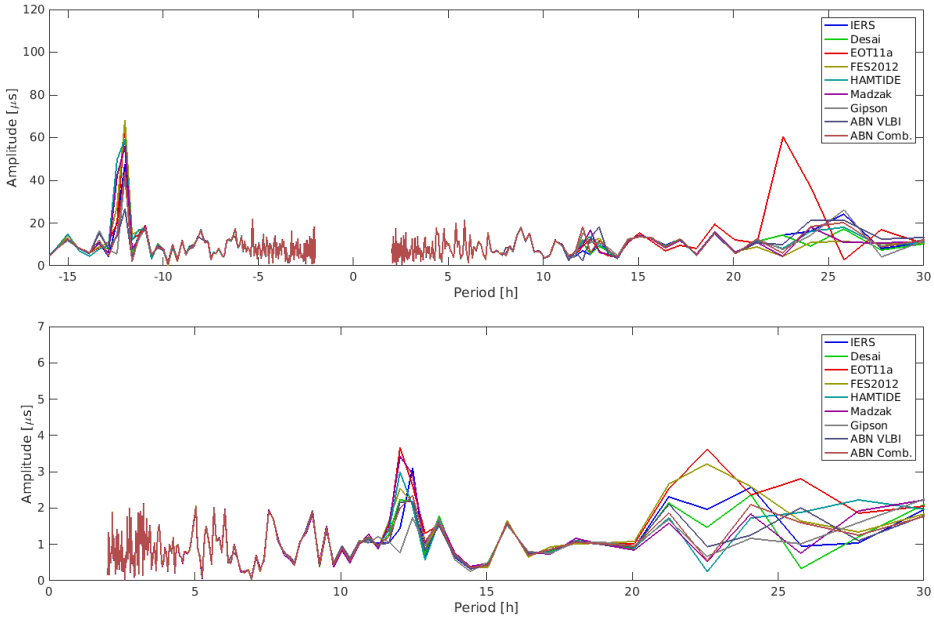

Figure 6: Spectra of the residual polar motion ($p = x_p - i\,y_p$, top) and UT1-UTC (bottom variations after the various models have been removed from the estimated EOP time series from the CONT11 campaign.

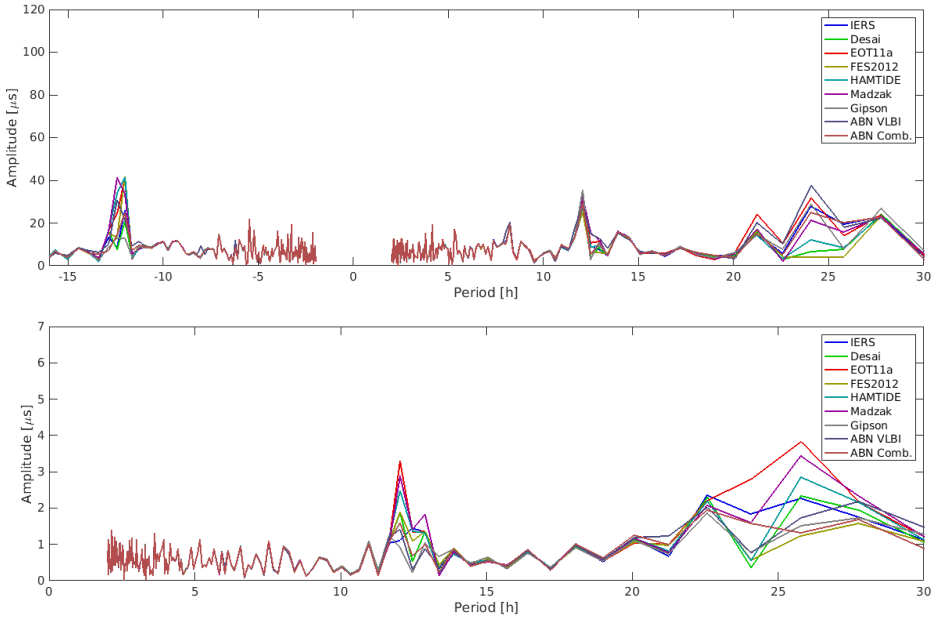

Figure 7: Spectra of the residual polar motion ($p = x_p - i\,y_p$, top) and UT1-UTC (bottom variations after the various models have been removed from the estimated EOP time series from the CONT14 campaign.

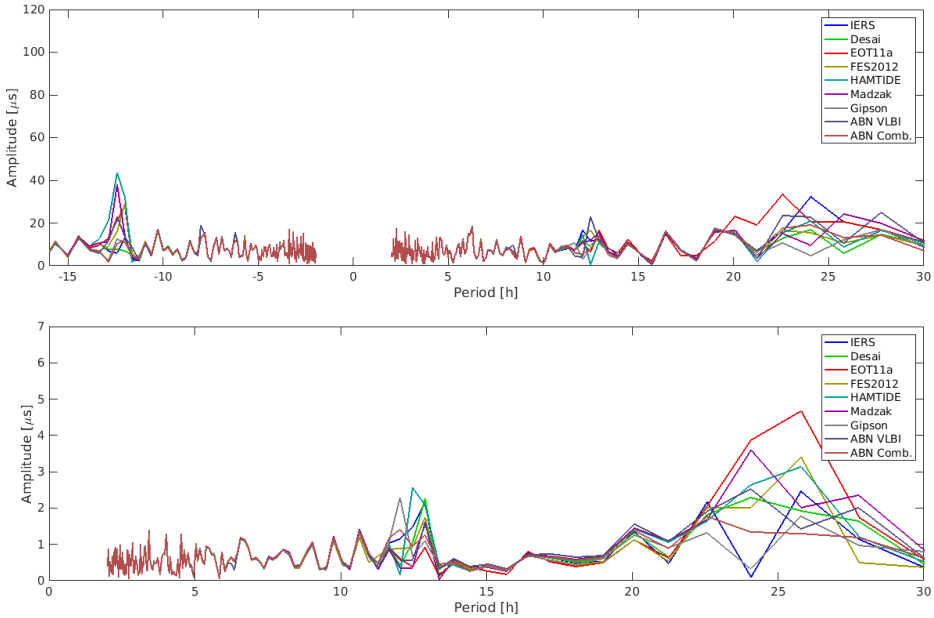

Figure 8: Spectra of the residual polar motion ($p = x_p - i\,y_p$, top) and UT1-UTC (bottom variations after the various models have been removed from the estimated EOP time series from the CONT17 campaign.

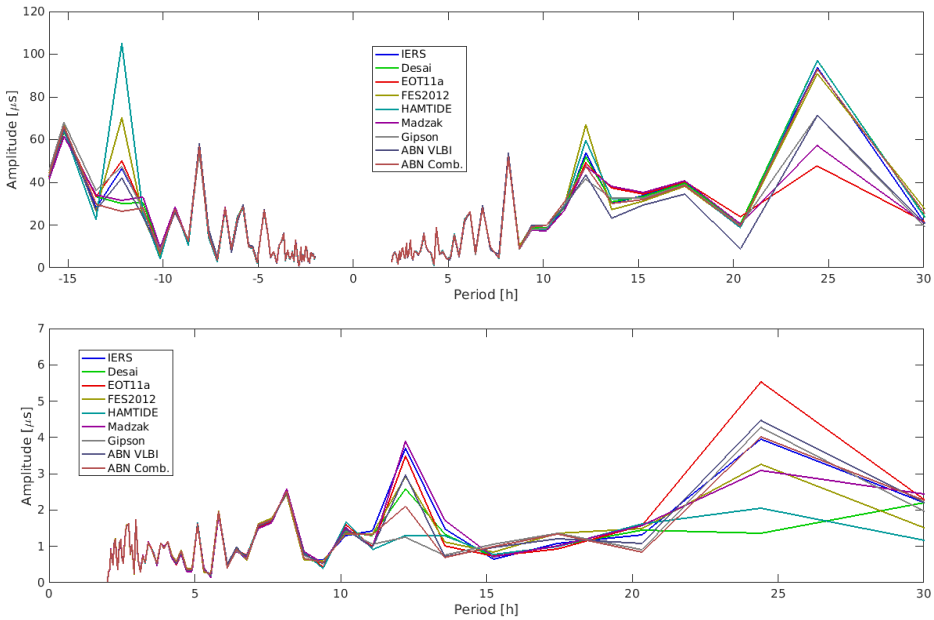

Figure 9: Spectra of the residual polar motion ($p = x_p - i\,y_p$, top) and UT1-UTC (bottom variations after the various models have been removed from the estimated EOP time series from the VGOS17 campaign.